International Journal of Geology, Earth & Environmental Sciences ISSN: 2277-2081
An Open Access, Online International Journal Available at http://www.cibtech.org/jgee.htm
2026 Vol. 16, pp. 17-32/Djerossem
Research Article

PETROGRAPHIC AND GEOCHEMICAL CHARACTERIZATION OF THE ABOUDEÏA GRANITOIDS (GUÉRA MASSIF, CHAD): IMPLICATIONS FOR MAGMA SOURCE AND TECTONIC SETTING

***F.N. Djerossem[1], M.N. Klamadji[2], P. Rondouba[1]**
[1]Department of Mining, New and Renewable Energies. National Higher Institute of the Sahara and Sahel, Iriba, Chad
[2]Department of Mining and Geological Engineering, Faculty of Life and Earth Sciences, Pala University, P.O. Box. 20, Pala, Chad
**Author for Correspondence*

ABSTRACT
The Aboudeïa locality, situated in the Guera massif, is part of the Central African Orogenic Belt (CAOB). Petrographic and geochemical investigations conducted in the Aboudeïa region have identified four main types of granitoids: monzonite (MZ), biotite granite (BG), biotite microgranite (BM) and leucogranite (LG). The monzonites exhibit a metaluminous character with a shoshonitic affinity, whereas BG, BM, and LG range from metaluminous to weakly peraluminous and display a high-K calc-alkaline affinity. All studied granitoids are characterized by positive anomalies in Rb and Th, enrichment in light rare earth elements (LREE), and pronounced negative anomalies in Ba, Nb, Ta, Eu, Sr, and Ti. These geochemical features suggest a magmatic origin involving partial melting of the continental crust, within various tectonic settings: volcanic arc for MZ, and syn-collisional to intraplate environments for BG, BM, and LG. Their evolution is mainly dominated by fractional crystallization, with possible mantle contamination linked to subduction processes. These characteristics indicate the presence of a former subduction zone, followed by a collisional episode and subsequent post-collisional tectonomagmatic reactivation. Collectively, the Aboudeïa granitoids constitute key evidence for reconstructing the geodynamic history of the Guéra Massif and the central Chad region within the broader framework of the Pan-African orogeny.

Keywords: *Central African Orogenic Belt, Guéra Massif, Aboudeïa, volcanic arc granite, syn-collisional granite, fractional crystallization*

1. INTRODUCTION

The Central African Orogenic Belt (CAOB), also known as the Central African Pan-African Belt or Central African Mobile Zone, represents a segment of continental crust reworked during the Pan-African orogeny, between 700 and 500 million years ago (Jackson and Ramsay, 1980; Bessoles and Trompette, 1980). This orogenic belt resulted from the convergence and collision of the West African and Congo–São Francisco cratons, along with the Saharan metacraton, during the assembly of Western Gondwana (Castaing *et al.,* 1994; Abdelsalam *et al.,* 2002). The CAOB extends across several Central African countries, including Cameroon, the Central African Republic, and Chad (Figure. 1a). It records a complex tectonic history marked by successive episodes of subduction, continental collision and crustal reactivation (Pham *et al.,* 2020).

In Chad, located in the northern part of the CAOB, granitoid massifs are distributed across several regions: Tibesti in the north, Ouaddaï in the east, Guéra in the center, Mayo Kebbi in the southwest, and Baïbokoum in the south (Figure. 1a). These massifs host post-collisional granitoids that represent the final stages of the Pan-African orogenic cycle (Pouclet *et al.,* 2006; Isseini *et al.,* 2012; Shellnutt *et al.,* 2018;

Djerossem *et al.,* 2020; Diontar *et al.,* 2020; Seguem *et al.,* 2022; Assadi *et al.,* 2022; Baïssemia Ronang *et al.,* 2024). Studies conducted in the Guéra Massif have revealed geochemical features typical of post-collisional granites, including crystallization under moderate temperatures and variable pressures, reflecting late magmatic evolution associated with tectonic relaxation (Shellnutt *et al.,* 2018; Pham *et al.,* 2020).

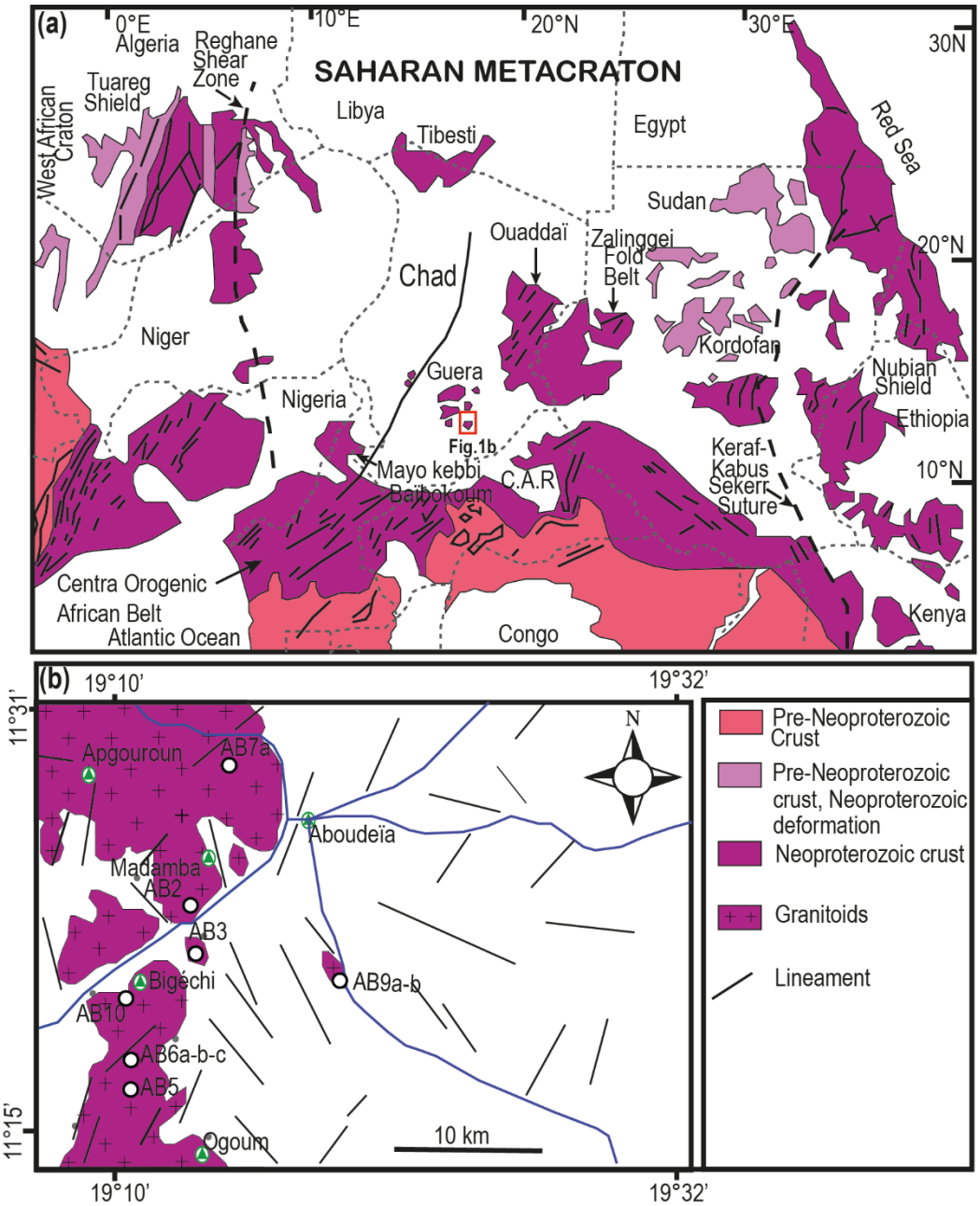

Figure 1. (a) Simplified geological map of the Saharan Metacraton, showing the location of the study areas modified from (Abdelsalam *et al.,* 2002). (b) Geological map of Aboudeïa.

The Aboudeïa area (figure. 1b), located in the southeastern part of the Guéra Massif, has been the subject of early petrographic investigations. However, these previous studies did not provide sufficient insight into the petrogenesis of the granitoids. The present study, based on petrographic observations and the

geochemistry of major and trace elements, aims to determine the nature, source, and tectonic setting responsible for the emplacement of the Aboudeïa granitoids.

2. GEOLOGICAL SETTING

Chad is a vast territory located in the heart of Africa, integrated into the Central African Orogenic Belt (CAOB; Kusnir and Moutaye, 1997), which extends northward into the Saharan Metacraton (Shellnutt *et al.,* 2018). According to Kasser (1995), the Precambrian basement formations of Chad are subdivided into two major domains, separated by a gravimetric anomaly (Louis, 1970; Braitenberg *et al.,* 2011). This anomaly represents the continuation of the Banyo–Tcholliré shear zone in Cameroon, crossing the Mayo Kebbi Massif in southwestern Chad, the Guéra Massif in the center, and gradually attenuating toward the Tibesti in the north (Figure. 1a). This lineament, oriented N–S to ENE–WSW (Braitenberg *et al.,* 2011; Liégeois et al 2013), is now considered a major structural feature of the Saharan Metacraton. It may correspond to the eastern boundary of the Chadian cratonic core, integrated into the Saharan Metacraton (Shellnutt *et al.,* 2018; Pham *et al.,* 2020).

The Guéra Massif, which is the focus of this study, is located in central Chad and represents the eastern domain of this suture. It is mainly composed of granitoids, crosscut by a weakly metamorphosed volcano-sedimentary sequence (Kusnir and Moutaye, 1997; Kasser, 1995). Recent investigations in this region have revealed the presence of fine-grained mafic enclaves, gabbros, diorites, granodiorites, biotite granites, and fine-grained granites (Isseini *et al.,* 2013; Shellnutt *et al.,* 2016; Pham *et al.,* 2020; Diontar *et al.,* 2020; Assadi *et al.,* 2022).

The gabbro–diorites and mafic enclaves are derived from mantle-origin magmas modified by subduction-related fluids (Shellnutt *et al.,* 2019; Diontar *et al.,* 2020). Their evolution is controlled by fractional crystallization processes, associated with crustal contamination.

Studies show that the Guéra granites display varied tectonic contexts. Biotite granites, ranging from metaluminous to peraluminous, with compositions from ferroan to magnesian and calc-alkaline affinity are distinguished (Le Maitre, 1989; Shellnutt *et al.,* 2019). The magnesian granites (595 ± 8 Ma) are similar to volcanic arc granites, whereas the ferroan granites (589 ± 6 Ma) are typical of syn-collisional granites. These formations correspond to the ancient basement of the Guéra Massif.

Finally, biotite–amphibole granites, ranging from peraluminous to metaluminous, calc-alkaline, and ferroan in composition, were emplaced in a post-collisional setting between 561 ± 6 Ma and 556 ± 7 Ma. These rocks correspond respectively to intermediate granites and younger granites.

1. ANALYTICAL METHODS

Geological field campaigns were conducted in Aboudeïa locality in the center of Chad. This phase enabled the macroscopic identification of rock facies and the collection of key lithological parameters, including color, texture, mineralogical composition, degree of alteration, and deformation features. A total of ten (10) fresh, unaltered samples were selected. These include two samples of monzonite, tree biotite granite, tree biotite microgranite and two leucogranite.

Rocks samples were sawed into chips for thin section preparation and trimmed to small blocks for geochemical investigations. About 200 to 500 g of each sample was crushed into a steel jaw crusher and then pulverized with an agate ball mill. Powders were digested using an alkali fusion procedure where the powder was mixed to lithium metaborate and melted to produce a glass pellet. The pellet was digested into diluted nitric acid before analyses. Analyses and digestions were made at the ALS Geochemistry-Loughrea (Irland). Prepared samples (0.100 g) are added to lithium metaborate/lithium tetraborate flux, mixed well and fused in a furnace at 1000°C. The resulting melt is then cooled and dissolved in 100 mL of 4% nitric acid/2% hydrochloric acid. This solution is then analysed by ICP-AES and the results are corrected for spectral inter-element interferences. Oxide concentration is calculated from the determined elemental concentration and the result is reported in that format. The Whole Rock analysis is determined in conjunction with a loss-on-ignition at 1000°C. The resulting data from both determinations are combined to produce a "total". For the determination of trace-elements, the samples were mixed well and

fused in a furnace at 1025°C. The resulting melt is then cooled and dissolved in an acid mixture containing nitric, hydrochloric and hydrofluoric acids. This solution is then analyzed by ICP–MS.

4. PETROGRAPHIC RESULTS OF PLUTONIC ROCKS FROM ABOUDEÏA

4.1. Monzonite (MZ)

The monzonite (MZ) occurs as decimetric to metric blocks and slabs. It displays a yellowish-grey weathering patina, with dimensions ranging from 1 to 5 cm (Figure. 2a, b). The rock is composed of feldspar, quartz, and ferromagnesian minerals (amphibole and biotite). It contains microgranular mafic enclaves and dolerite, and is crosscut by quartz–feldspar pegmatite veins. The stretching of minerals such as biotite indicates deformation during emplacement. In thin section, the monzonite exhibits a coarse-grained porphyroid texture (Figure. 3a). The mineral assemblage consists of K-feldspar, plagioclase, quartz, biotite, clinopyroxene, amphibole, and accessory phases (sphene, epidote, and oxides). K-feldspar (~40%) is xenomorphic, occurring as large, partly altered patches that enclose inclusions of biotite and plagioclase. Plagioclase (~35%) appears as large xenomorphic crystals, occasionally associated with small quartz crystals (~10%), and also occurs as inclusions within K-feldspar phenocrysts. Quartz is present as small elongated grains or as large lobate patches. Biotite (~8%) occurs as elongated flakes. Clinopyroxene (<5%) is moderately elongated and shows well-developed cleavage. Amphibole (<5%) is less abundant, occurring as small crystals associated with plagioclase and quartz. Numerous oxide inclusions are observed within altered crystals. Sphene, epidote, and oxides are accessory minerals (<2%), occurring as minor intrusions.

4.2. Biotite Granite (BG)

Biotite granites (BG) are predominant in the study area, occurring as blocks and boulders (Figure. 2c, d). At the outcrop scale, BG display a dark to grey coloration due to weathering, and are crosscut by quartz–feldspar veins while containing mafic enclaves. They are not in direct contact with the monzonite (MZ), but show comparable deformation features.

In thin section, biotite granites exhibit a coarse-grained porphyroid texture (Figure. 3b). The mineral assemblage consists of K-feldspar, quartz, plagioclase, biotite, and oxides. K-feldspar (~45%) occurs as large, partly altered crystals enclosing inclusions of biotite and oxides. Quartz (~30%) forms irregular crystals, locally marked by lobate margins indicative of high-temperature recrystallization. Plagioclase (~15%) appears as sub- to euhedral crystals associated with K-feldspar and quartz. Biotite (~10%) occurs as lamellae within the interstices of K-feldspar and quartz, and contains inclusions of opaque minerals.

4.3. Biotite Microgranite (BM)

Biotite microgranites (BM) crop out as metric to decametric boulders and blocks in Aboudeïa and its surroundings (Figure. 2e, f). At the outcrop scale, BM displays a yellowish coloration due to weathering patina. The rock mass is affected by microfractures that break it into boulders or blocks. BM occasionally occurs as dykes or veins crosscutting the biotite granites (BG) and leucogranites (LG).

In thin section, biotite microgranites exhibit a fine-grained texture (Figure. 3c). The mineral assemblage consists of quartz, alkali feldspar, plagioclase, biotite, and minor accessory phases such as zircon, pyrite, and opaque minerals. Quartz (~45%) is xenomorphic and occurs in two generations: the first generation forms large lobate patches, while the second generation is represented by neograins filling the interstices between K-feldspar and plagioclase phenocrysts. K-feldspar (~25%) occurs as altered phenocrysts enclosing inclusions of biotite and plagioclase. Plagioclase (~15%) is present as xenomorphic crystals, partly altered, associated with quartz and biotite, and containing inclusions of biotite. Biotite (~5%) occurs as elongated patches, associated with quartz and plagioclase, and occasionally enclosing inclusions of oxides and zircon (<2%).

4.4. Leucogranite (LG)

Leucogranites (LG) crop out as slabs (Figure. 2g, h). These rocks are whitish in color and are predominantly composed of quartz, plagioclase, muscovite, and biotite, which are visible to the naked eye. The rock is crosscut by fine-grained granite veins oriented E–W.

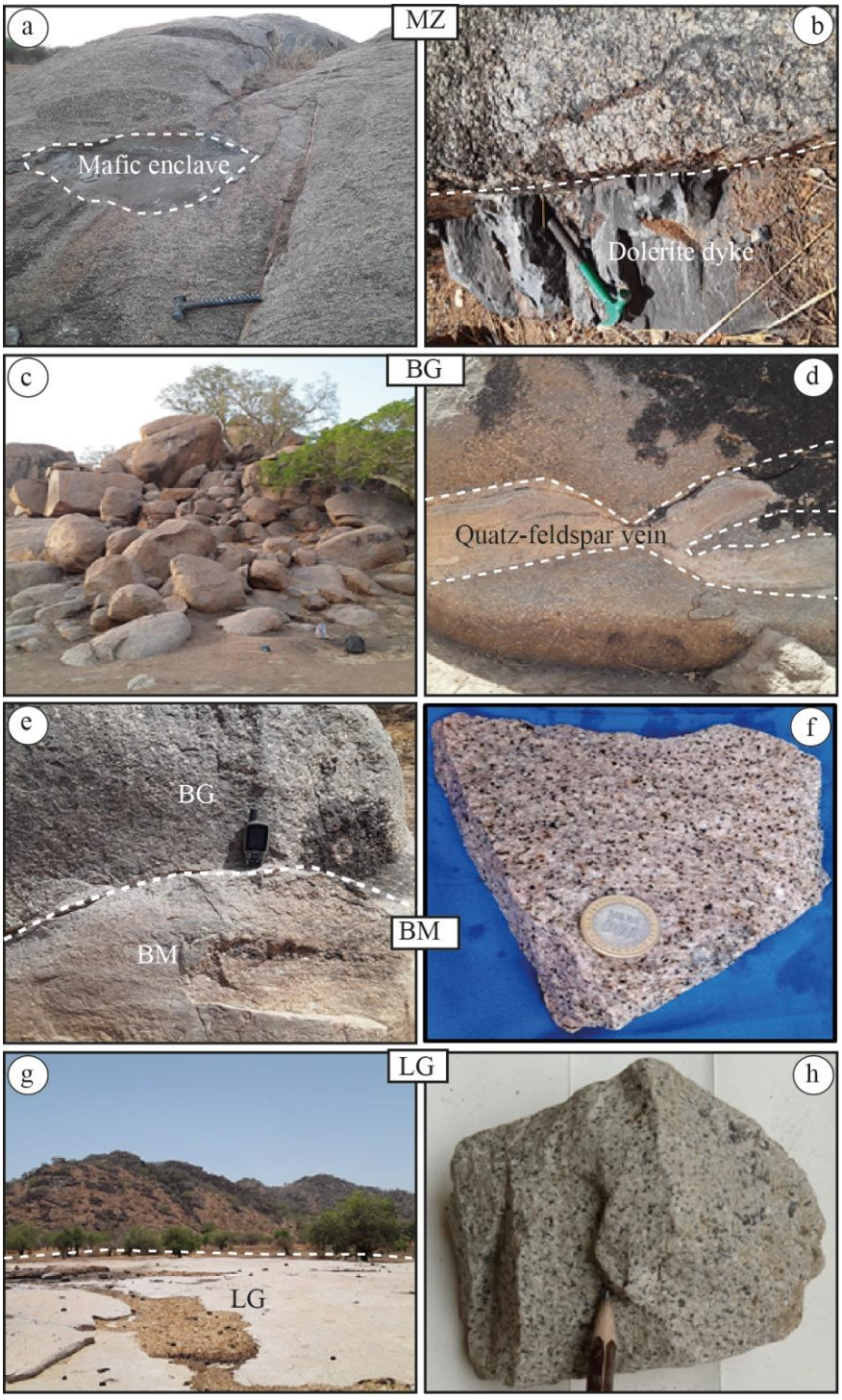

Figure 2. Field views of the Aboudeïa granitoids. (a) and (b) Outcrop and photographs of monzonite (MZ), crosscut by a mafic enclave and a dolerite dyke. (c) and (d) Outcrop photographs of biotite granite (BG), crosscut by a quartz–feldspar vein. (e) and (f) Outcrop and photographs of biotite microgranite (BM) in sharp contact with biotite granite. (g) and (h) Slab outcrop of leucogranite (LG).

In thin section, leucogranite exhibits a coarse-grained texture (Figure. 3d). It is largely composed of leucocratic minerals such as K-feldspar, quartz, and plagioclase, with minor biotite crystals. Accessory minerals are represented by opaque phases. K-feldspar (~45%) occurs as large elongated xenomorphic patches, forming the bulk of the rock. Quartz (~30%) ranges from euhedral to xenomorphic, and occasionally occurs as inclusions within plagioclase crystals. Plagioclase (~12%) is xenomorphic and characterized by polysynthetic twinning. Biotite (~10%), brown in color, occurs as small elongated flakes, representing a minor proportion of the rock-forming minerals. Oxides (~2%) are generally interstitial and occur as inclusions within feldspar crystals.

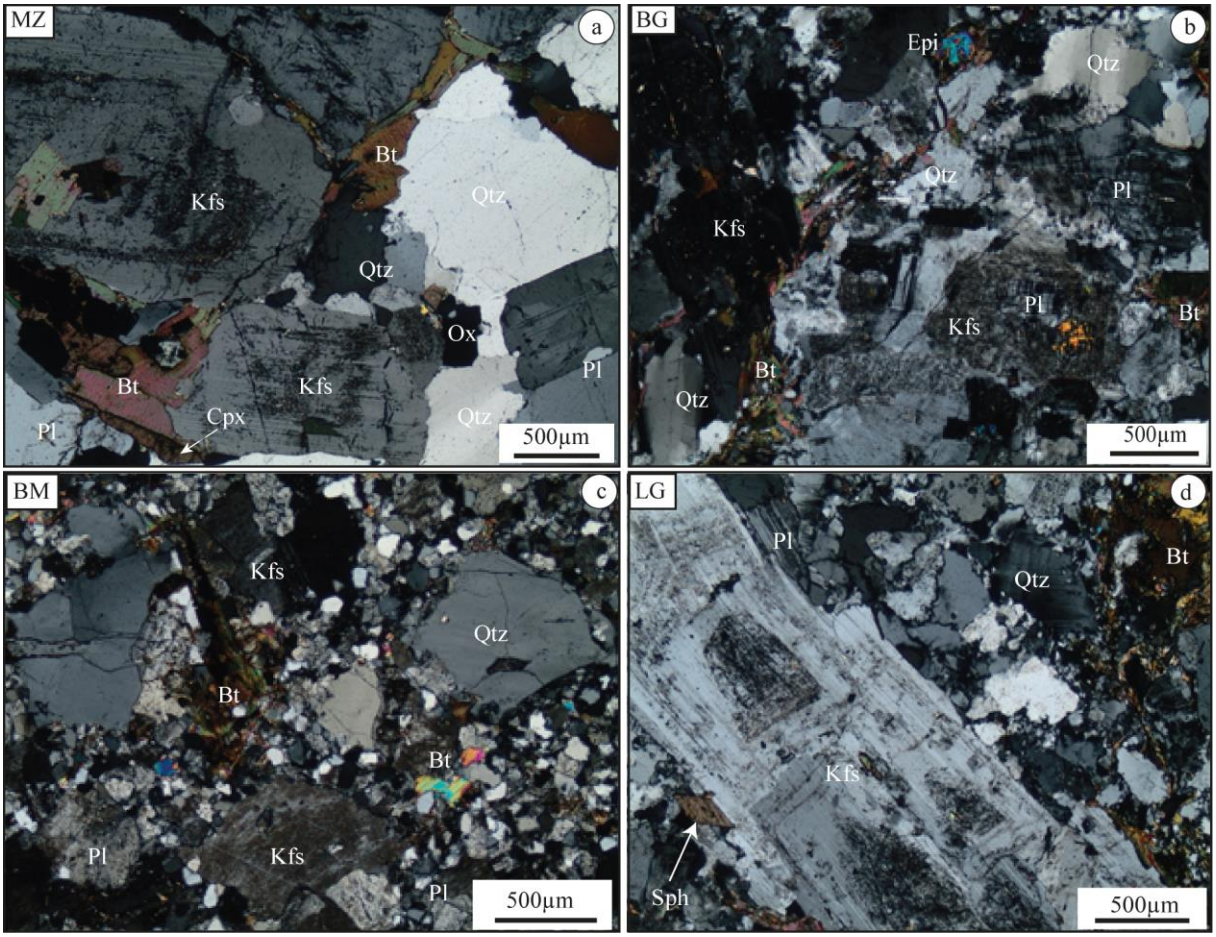

Figure 3. Representative photomicrographs of thin sections of the granitoids. (a) Coarse-grained texture of monzonite (MZ) rich in quartz. (b) Photomicrograph of biotite granite (BG). (c) Fine-grained texture of biotite microgranite (BM). (d) Coarse-grained texture of leucogranite (LG).

5. GEOCHEMICAL RESULTS OF PLUTONIC ROCKS FROM ABOUDEÏA

5.1. Major and Trace Elements

The geochemical compositions (major and trace elements) of the plutonic rocks from the study area are presented in Table. 1. These data are plotted in binary diagrams, rare earth element (REE) diagrams, and multi-element diagrams to identify the main magmatic trends of these rocks. Four petrographic types are generally studied: monzonite (MZ), biotite granite (BG), biotite microgranite (BM), and leucogranite (LG). In Harker-type diagrams (oxide vs. SiO_2), the Aboudeïa granitoids show negative linear

correlations for Fe_2O_3, TiO_2, MnO, MgO, P_2O_5, Al_2O_3, CaO, and Na_2O with increasing SiO_2 content (Figure. 5).

Table 1. Major (wt%) and trace elements (in ppm) compositions for the Aboudeïa granitoïds

	Monzonite		Biotite granite			Biotite microgranite			Leucogranite	
Sample	AB6	AB10	AB7a	AB3	AB6a	AB9	AB6b	AB9a	AB2	AB5
SiO_2	66.60	66.20	70.80	75.10	74.00	74.20	73.00	75.00	73.70	74.00
Al_2O_3	15.40	15.20	13.45	12.75	13.10	13.00	12.95	13.50	12.85	12.64
Fe_2O_3	4.57	4.71	4.17	1.92	2.38	2.73	3.10	2.11	3.10	3.07
CaO	2.33	2.36	1.56	1.08	1.40	1.06	1.01	1.03	1.09	1.20
MgO	0.84	0.82	0.29	0.21	0.19	0.21	0.25	0.10	0.15	0.18
Na_2O	3.69	3.72	3.34	3.27	3.11	3.10	3.90	3.03	3.01	3.50
K_2O	5.01	4.77	4.96	4.57	4.26	5.34	4.41	5.08	5.32	4.77
Cr_2O_3	0.02	0.02	0.02	0.03	0.03	0.02	0.06	0.10	0.02	0.03
TiO_2	0.70	0.70	0.41	0.21	0.19	0.32	0.22	0.36	0.28	0.30
MnO	0.06	0.06	0.07	0.03	0.05	0.04	0.03	0.05	0.04	0.04
P_2O_5	0.24	0.25	0.11	0.04	0.09	0.04	0.02	0.07	0.05	0.02
SrO	0.05	0.05	0.02	0.03	0.01	0.02	0.01	0.04	0.02	0.04
BaO	0.17	0.17	0.11	0.06	0.09	0.09	0.05	0.10	0.08	0.05
LOI	0.65	0.77	0.38	0.57	0.41	0.76	0.29	0.82	0.66	0.53
Total	100.33	99.80	99.69	99.87	99.31	100.93	99.30	101.39	100.37	100.72
Na_2O+K_2O	8.70	8.49	8.30	7.84	7.37	8.44	8.31	8.11	8.33	8.27
Mg#	26.83	25.78	12.18	17.91	13.74	13.30	13.86	8.64	8.80	10.47
FeOt	4.11	4.24	3.75	1.73	2.14	2.46	2.79	1.90	2.79	2.76
A/NK	1.34	1.35	1.24	1.23	1.35	1.19	1.16	1.29	1.20	1.16
A/CNK	0.98	0.98	0.98	1.04	1.07	1.02	0.99	1.09	1.01	0.96
Sc	5.90	5.40	5.80	1.10	4.20	3.40	2.10	3.02	3.70	3.21
V	34.00	36.00	10.00	5.00	6.12	11.00	3.40	2.87	<5	4.03
Cr	130.00	168.00	173.00	227.00	222.00	152.00	162.00	149.00	172.00	180.00
Rb	147.00	141.00	272.00	196.00	215.00	244.00	235.00	218.00	283.00	277.00
Sr	386.00	384.00	151.00	152.50	150.00	89.90	91.09	82.90	89.20	90.30
Zr	525.00	526.00	553.00	183.00	287.00	423.00	417.00	397.00	485.00	456.00
Nb	28.70	29.70	34.30	22.80	30.00	34.10	29.00	33.40	40.80	40.80
Cs	0.51	0.52	3.83	0.62	2.90	2.12	2.54	2.46	2.92	2.80
Ba	1590.00	1525.00	1005.00	519.00	851.00	792.00	634.00	765.00	770.00	745.00
Y	21.50	22.00	63.40	13.60	59.00	52.70	50.50	49.80	78.40	76.80
La	166.50	160.50	111.00	60.40	70.30	59.20	60.10	48.40	155.00	149.60
Ce	300.00	293.00	235.00	113.00	110.00	132.50	122.00	129.00	324.00	290.00
Pr	28.30	27.80	26.30	11.30	15.60	15.70	14.50	12.70	35.70	30.30
Nd	92.00	88.40	98.50	35.00	77.50	59.40	50.50	49.80	128.00	123.10
Sm	12.40	12.40	18.45	5.13	10.30	12.65	11.40	14.50	22.60	19.60
Eu	2.24	2.20	2.21	1.30	1.13	1.17	1.20	1.24	1.59	1.32
Gd	7.71	7.94	15.00	3.32	7.33	10.65	9.21	7.98	17.10	13.60
Tb	0.92	0.93	2.08	0.43	1.90	1.59	1.14	1.39	2.40	2.11
Dy	4.79	4.83	12.10	2.40	6.20	9.31	9.04	7.66	14.15	13.56
Ho	0.82	0.78	2.30	0.43	1.80	1.81	1.50	1.77	2.77	2.39
Er	2.02	1.99	6.44	1.20	5.10	5.22	4.78	5.03	7.58	6.23
Tm	0.23	0.26	0.86	0.19	0.53	0.77	0.45	0.33	1.06	0.99
Yb	1.56	1.50	5.52	1.19	3.40	5.01	2.34	4.10	6.94	5.62
Lu	0.23	0.23	0.82	0.16	0.24	0.75	0.42	0.65	1.03	1.14
Hf	11.70	11.90	13.70	5.26	7.70	11.05	8.23	7.41	13.20	12.20
Ta	1.40	1.50	2.20	2.30	2.07	2.00	1.99	2.09	2.90	2.54
W	1.00	0.80	1.30	0.70	1.O5	1.10	0.79	1.18	1.60	1.15
Th	29.00	28.00	26.60	54.90	33.00	27.20	25.00	26.76	39.30	28.56
U	1.47	1.47	3.13	7.81	2.70	3.13	3.04	2.48	4.33	3.90
Ga	25.50	25.80	25.60	22.20	21.70	21.90	22.01	21.70	24.10	23.40

5.1.1. Monzonite (MZ)

MZ samples exhibit relatively low SiO_2 contents (62.2–66.6 wt.%) compared to other lithologies. K_2O (4.77–5.01 wt.%) and Na_2O (3.69–3.72 wt.%) contents are moderately variable, with K_2O/Na_2O ratios ranging from 1.28 to 1.37. Total alkali contents ($Na_2O + K_2O$) range between 6.13 and 6.37 wt.%. In the (Sun and McLennan 1989), classification diagram (Figue. 4a), MZ corresponds to quartz monzonite. It displays a shoshonitic affinity (Fig 4b) and belongs to the calc-alkaline series (Figure. 4c). These rocks

are metaluminous I-type granitoids, as indicated by molar ratios A/CNK ($Al_2O/[CaO + Na_2O + K_2O]$) and A/NK ($Al_2O_3/ [Na_2O + K_2O]$), ranging from 0.97–0.98 and 1.33–1.35, respectively (Figure. 4d). MZ also shows high Na_2O_3 (15.2–15.4 wt.%) and low Fe_2O_3 (4.57–4.71 wt.%), CaO (2.33–2.36 wt.%), MgO (0.82–0.84 wt.%), and TiO_2 (0.7 wt.%). In the chondrite-normalized REE diagram (Figure. 6a), MZ is enriched in light rare earth elements (LREE) ($(La/Yb)_N$ = 76.55–76.75) relative to heavy rare earth elements (HREE) ($(La/Sm)_N$ = 8.35–8.67), and displays negative Eu anomalies (Eu/Eu* = 0.67–0.70). In the primitive mantle-normalized multi-element diagram (Figure. 6b; Sun and McLennan 1989), MZ shows negative anomalies in Ba, Nb, Ta, Sr, and Ti, with progressively decreasing HREE and enrichment in Th.

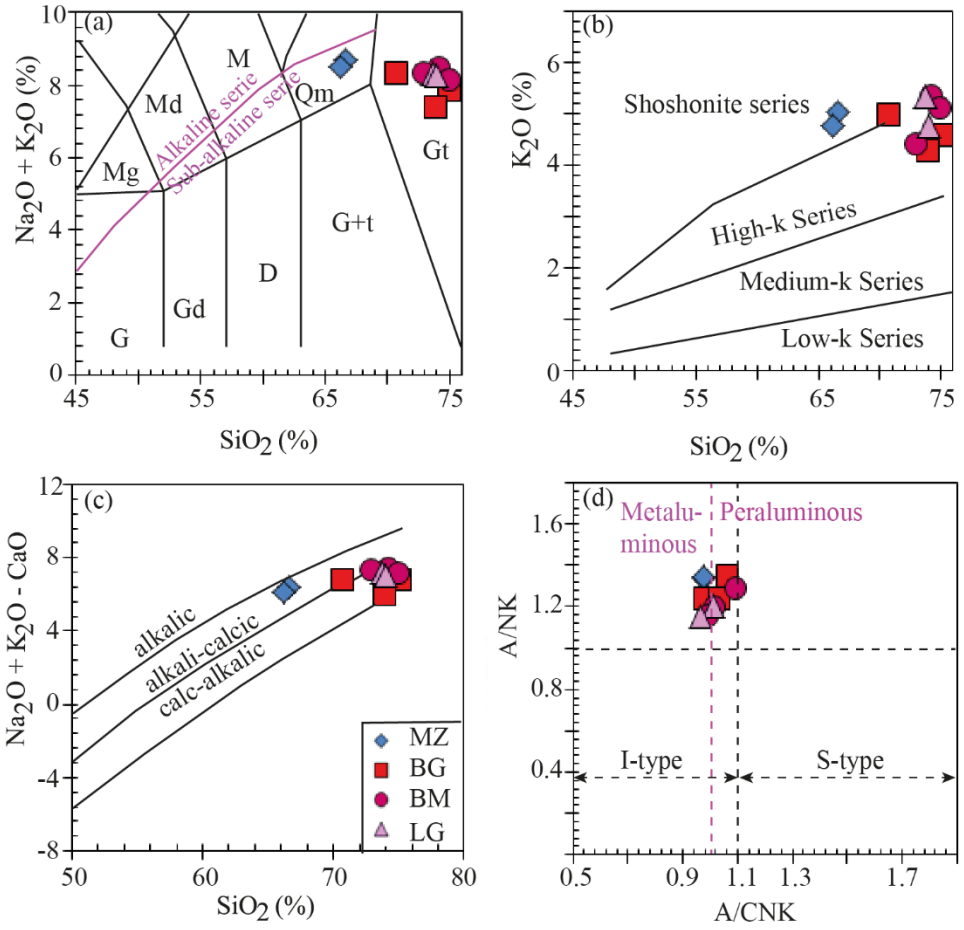

Figure 4. Geochemical classification of Aboudeïa granitoids: (a) SiO2 vs. Na2O + K2O diagram of (Le Maitre, 1989); (b) K2O vs. SiO2 diagram illustrating the low and high-K calc-alkaline affinities (Le Maitre, 1989; Rickwood, 1989); (c) SiO2 vs. Na2O + K2O - CaO diagram (Maniar and Piccoli, 1989); (d) A/NK = Al2O3/(Na2O+K2O) vs. A/CNK = Al2O3/(CaO+Na2O+K2O) (Maniar and Piccoli, 1989). Dashed line represents boundary between I- and S-type granites (Chappell and White, 1992). G (Gabbro), GD (Gabbro Diorite), D (Diorite), G+t (Granodiorite+tonalite), Gt (Granite), Gg (Monzogabbro), Md (Monzodiorite), M (Monzonite) et Qm (Monzonite quartzeux).

5.1.2. Biotite Granite (BG)

BG samples have slightly higher SiO_2 contents (70.8–75.1 wt.%) than MZ. Na_2O, K_2O and total alkalis ($Na_2O + K_2O$) range from 3.11–3.34 wt.%, 4.26–4.96 wt.%, and 7.37–8.30 wt.%, respectively. K_2O/Na_2O

ratios vary from 1.36 to 1.49. BG displays a strongly potassic to shoshonitic calc-alkaline affinity (Figure. 4b) and corresponds to metaluminous to weakly peraluminous I-type granitoids, with A/CNK and A/NK ratios ranging from 0.98–1.06 and 1.23–1.35 (Figure. 4d). Al_2O_{33} contents (12.75–13.45 wt.%) are lower than in MZ, and Fe_2O_{33} (1.92–4.17 wt.%), CaO (1.08–1.56 wt.%), MgO (0.19–0.29 wt.%), and TiO_{22} (0.19–0.41 wt.%) are also low. In the chondrite-normalized REE diagram (Figure. 6c), BG is enriched in LREE $((La/Yb)_N$ = 14.42–36.41) relative to HREE $((La/Sm)_N$ = 3.88–7.60), with negative Eu anomalies (Eu/Eu* = 0.39–0.96). In the primitive mantle-normalized diagram (Figure. 6d), BG shows negative anomalies in Ba, Nb, Ta, Sr, and Ti, and is enriched in Th with flat HREE patterns.

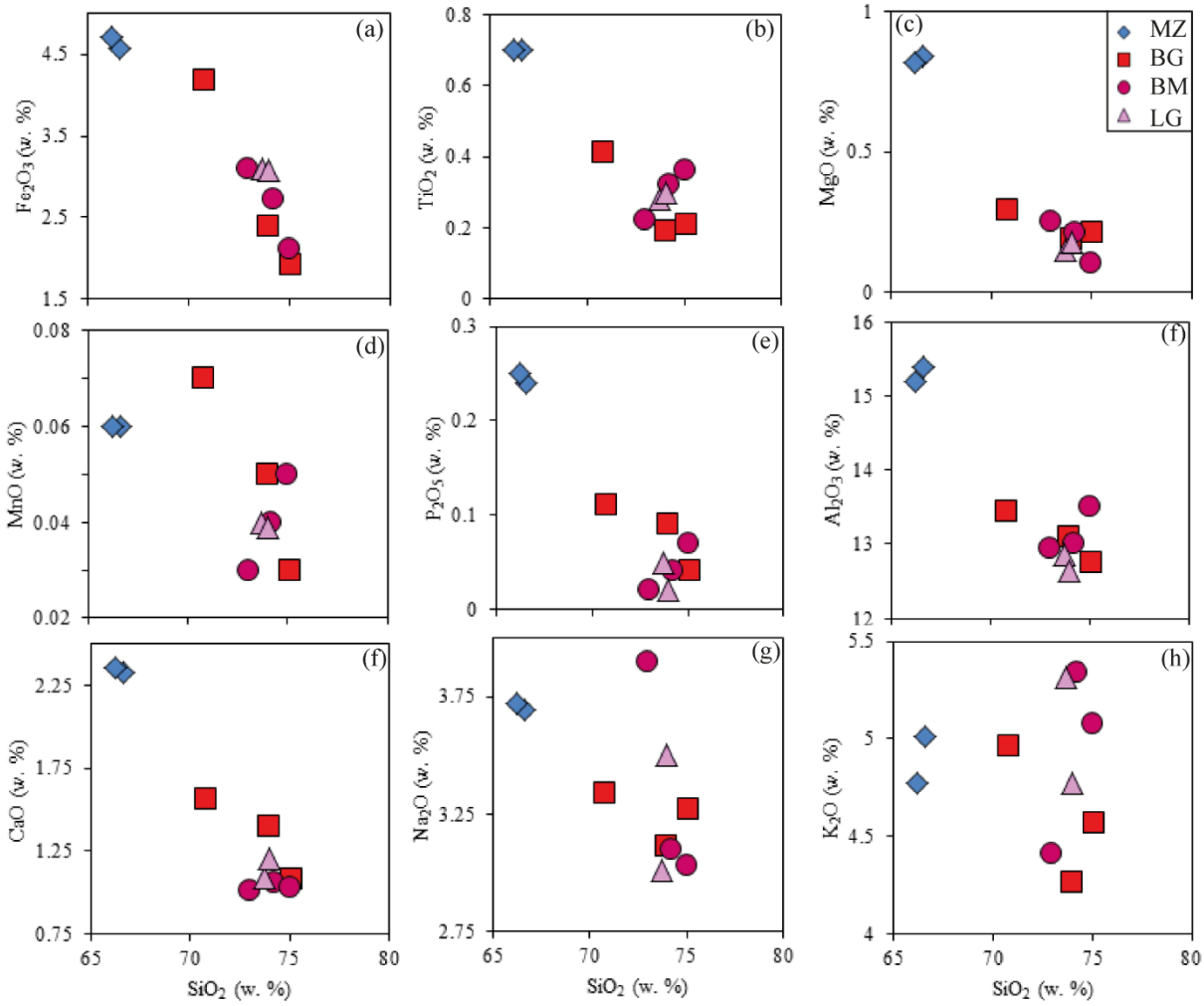

Figure 5. Distribution of the granitoids in the Harker diagram (oxides vs. SiO2 in wt. %).

5.1.3. Biotite Microgranite (BM)

BM samples have SiO_{22} contents of 73–75 wt.%, with K_2O (4.41–5.34 wt.%) and Na_2O (3.03–3.90 wt.%) similar to BG. K_2O/Na_2O ratios range from 1.13 to 1.72, and total alkalis range from 7.08 to 7.38 wt.%. BM displays a strongly potassic calc-alkaline affinity (Figure. 4b) and corresponds to weakly metaluminous to peraluminous I-type granitoids, with A/CNK and A/NK ratios between 0.99–1.09 and 1.15–1.29 (Figure. 4d). Al_2O_{33} contents (12.95–13.5 wt.%) are similar to BG, while Fe_2O_{33} (2.11–3.1 wt.%), CaO (1.01–1.06 wt.%), MgO (0.1–0.25 wt.%), and TiO_{22} (0.22–0.36 wt.%) remain low. In the chondrite-normalized REE diagram (Figure. 6e), BM is enriched in LREE $((La/Yb)_N$ = 8.47–18.42) relative to HREE $((La/Sm)_N$ = 2.15–3.40), with negative Eu anomalies (Eu/Eu* = 0.30–0.36). In the

primitive mantle-normalized diagram (Figure. 6f), BM shows negative anomalies in Ba, Nb, Ta, Sr, and Ti, and is enriched in Th with flat HREE profiles.

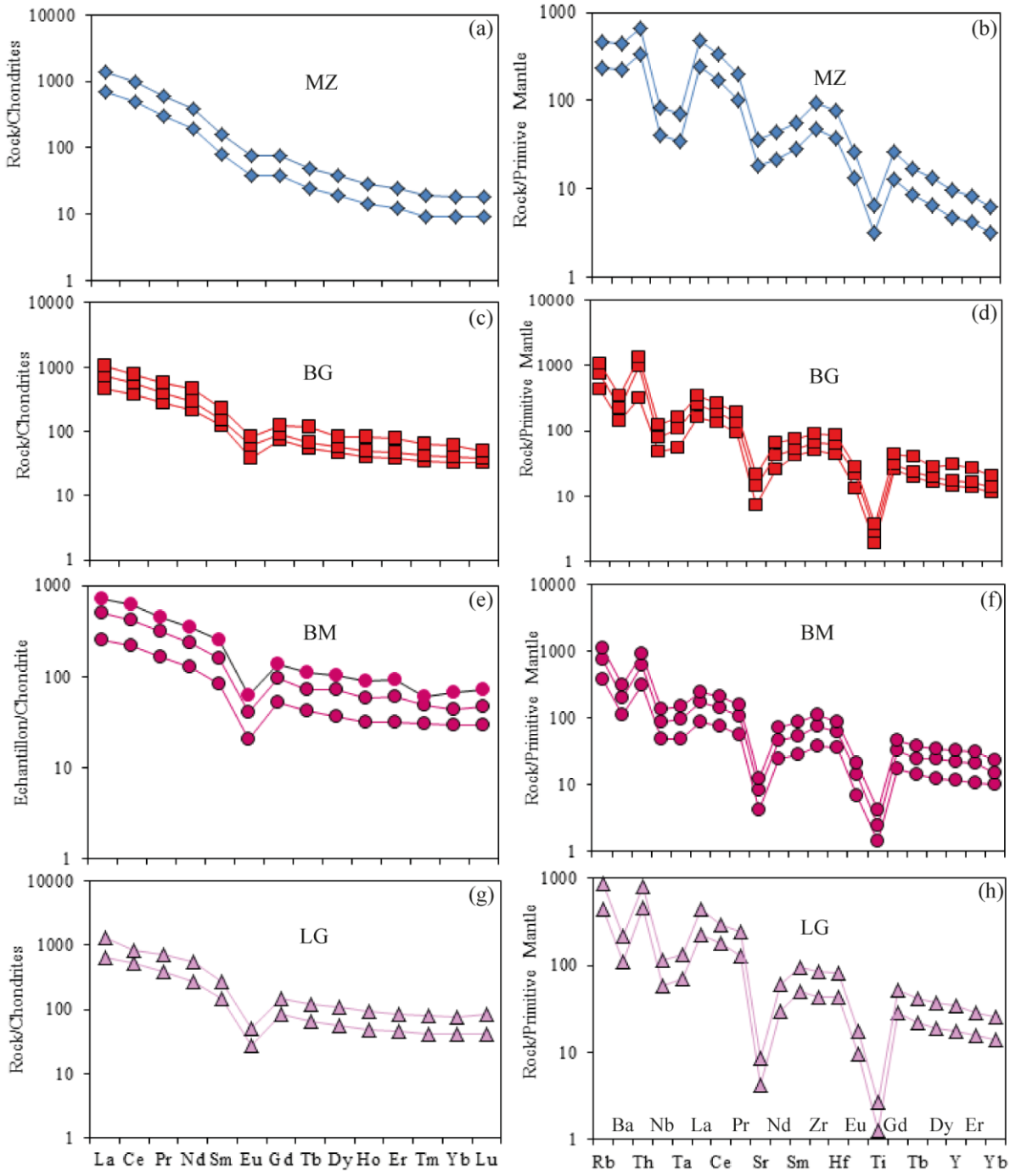

Figure 6. Chondrite-normalized REE patterns and primitive-mantle-normalized trace element spider diagrams of Aboudeïa granitoids after (Sun and McLennan 1989).

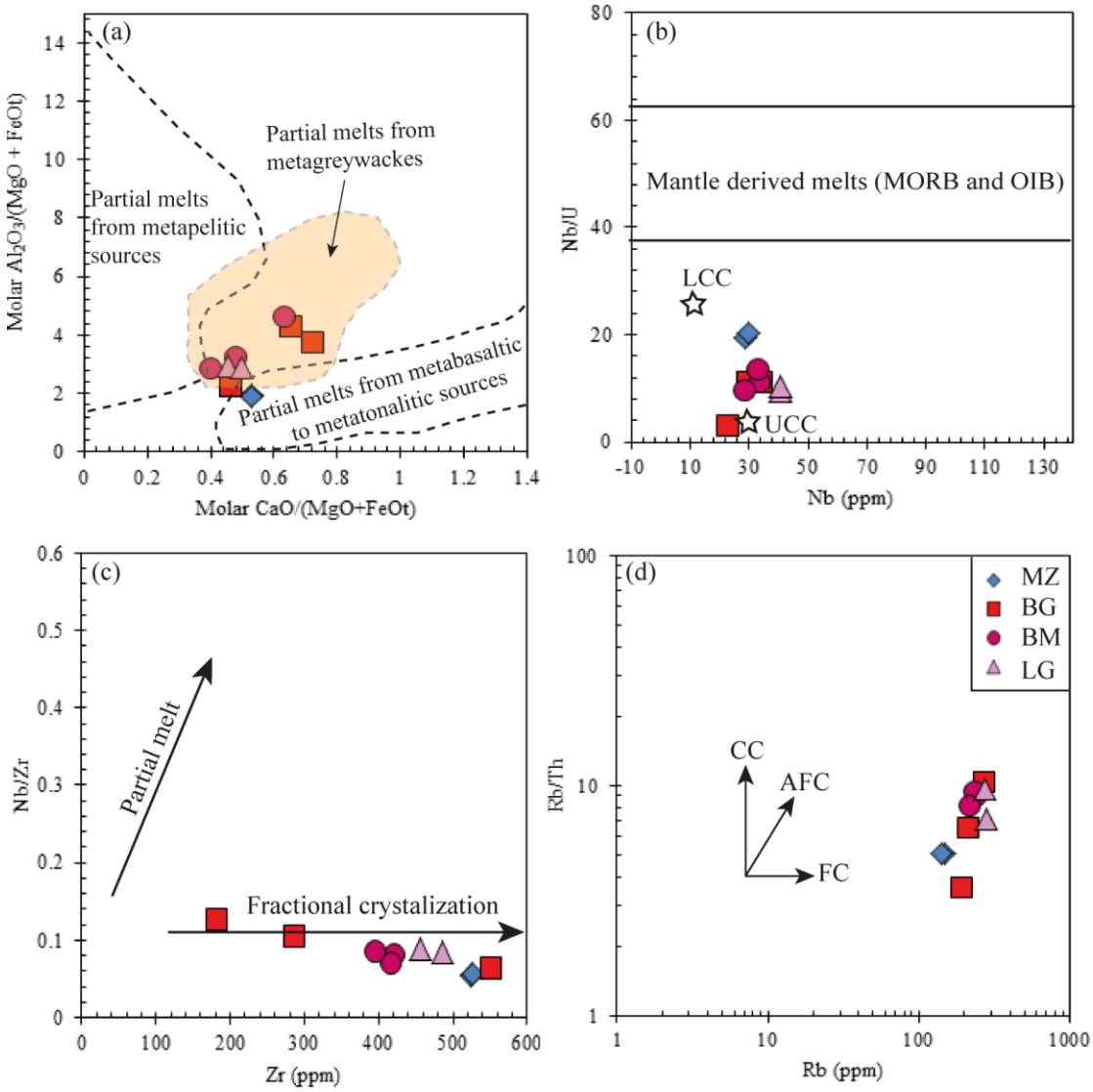

Figure 7. Sources and tectonic discrimionation diagram of the Aboudeïa granitoids: (a) Molar CaO/(MgO + FeOt) vs Al2O3/(MgO + FeOt); (b) Nb vs Nb/U. (c) Zr vs Nb/Zr and Rb vs Rb/Th. CC= Crustal Contamination; AFC= Assimilation Fractional Cristallization ; FC= Fractional Cristallization.

5.1.4. Leucogranite (LG)

LG samples show SiO_{22} contents of 73.7–74 wt.%, similar to BG and BM. Total alkali contents (Na_2O + K_2O) range from 8.27 to 8.33 wt.%. LG displays a strongly potassic calc-alkaline affinity (Figure. 4b) and corresponds to weakly metaluminous to peraluminous I-type granitoids, with A/CNK and A/NK ratios between 0.96–1.01 and 1.15–1.20 (Figure. 4d). Al_2O_{33} contents (12.64–12.85 wt.%) are comparable to BG and BM, while Fe_2O_{33} (3.07–3.1 wt.%), CaO (1.09–1.2 wt.%), MgO (0.15–0.18 wt.%), and TiO_{22} (0.28–0.3 wt.%) remain low. In the chondrite-normalized REE diagram (Figure. 6g), LG is enriched in LREE ($(La/Yb)_N$ = 16.02–19.09) relative to HREE ($(La/Sm)_N$ = 4.42–4.93), with a negative Eu anomaly (Eu/Eu* = 0.25). In the primitive mantle-normalized diagram (Figure. 6h), LG shows negative anomalies in Ba, Nb, Ta, Sr, and Ti, and a positive anomaly in Th.

DISCUSION

6.1. Nature and Sources of the Aboudeïa Granitoids

Understanding the source and tectonic environment of granitoids has crucial implications for continental crustal growth within the Central African Orogenic Belt (CAOB) in general, and within the Guéra Massif in particular. The Aboudeïa granitoids, represented by monzonite (MZ), biotite granite (BG), biotite microgranite (BM), and leucogranite (LG), are characterized by A/CNK ratios ranging from 0.96 to 1.09, typical of metaluminous to weakly peraluminous I-type granites (Chappell and White, 1974; Barbarin, 1999). Their elevated K_2O contents (4.26–5.34 wt.%) indicate a calc-alkaline to shoshonitic affinity. The molar ratio CaO/(MgO + FeOt) versus Al_2O_3/(MgO + FeOt) (Altherr *et al.,* 2000) further highlights the diversity of source rocks that underwent partial melting to produce these granitoids. In this diagram (Figure. 7a), MZ are derived from partial melting of metabasalts and metatonalites. Two BG samples, along with BM and LG, plot within the field of granitoids generated by partial melting of metagreywackes, while one BG sample falls between these two sources. This interpretation is consistent with the Nb/U vs Nb diagram, where BG, BM, and LG plot close to the upper continental crust (UCC), whereas MZ are closer to the lower continental crust (LCC; Figure. 7c). Low V contents and Mg# values, together with low Nb/U and Ta/U ratios, reflect a crustal signature (Hofmann *et al.,* 1997; Wu *et al.,* 2020). However, these granitoids also display high Cr contents (>151 ppm), coupled with negative anomalies in Ba, Nb, Ta, and Ti, which are typical of mantle-derived magmas (Hofmann *et al.,* 1997; Wu *et al.,* 2020). These mixed geochemical features support the hypothesis of partial melting of a metasomatized mantle, coupled with crustal contamination (Moyen *et al.,* 2017).

In the Arker diagram (Figure. 5), all granitoids show negative linear correlations with increasing SiO_2 content (Al_2O_3, TiO_2, Fe_2O_3, MgO, CaO, Na_2O, and P_2O_5). These correlations play an important role in the crystallization of mineral phases. Decreases in Al_2O_3 and CaO with increasing SiO_2 are linked to plagioclase and apatite fractionation. This plagioclase fractionation is further evidenced by pronounced negative Eu and Sr anomalies. Decreases in Na_2O and K_2O with increasing SiO_2 reflect feldspar fractionation. Decreases in Fe_2O_3, TiO_2, MnO, MgO, and P_2O_5 with increasing SiO_2 are related to fractionation of magnetite, ilmenite, titanite, amphibole, biotite, and apatite. These successive mineral fractionation processes confirm that fractional crystallization was the dominant mechanism during the emplacement of these granitoids. This is further supported by the parallelism of rare earth element (REE) spectra (Figure. 6) and by the consistency of immobile element ratios (Nb/Zr vs Zr), where all granitoids plot along the fractional crystallization trend (Figure. 7c), probably associated with crustal assimilation as indicated in the Rb/Th vs Rb diagram (Figure. 7d).

6.2. Tectonic Environment of the Aboudeïa Granitoids

In the Rb vs (Yb + Ta) diagram (figure 8a), the monzonites plot within the field characteristic of volcanic arc granites, whereas the biotite granites and biotite microgranites fall into the syn-collisional granite domain, typical of ancient basement granites as described respectively in the Ngoura and Bitkine localities (Guera Massif) (Shellnutt *et al.,* 2018; Pham *et al.,* 2020).

However, the calc-alkaline affinity with a strongly potassic to shoshonitic trend, combined with pronounced negative anomalies in Nb, Ta, and Ti across the granitoid suite, indicates a lithospheric convergence tectonic setting, consistent with the works of (Pearce (1975); Thompson *et al.,* 1984, Pouclet *et al.,* 2006). Moreover, the high ratios of incompatible trace elements Nb/Ta (9.91 to 20.5), La/Nb (1.44 to 5.80), and La/Ta (29.60 to 118.92), associated with low Rb contents; suggest a magmatic origin related to a subduction environment. In the Zr vs (Nb/Zr)N diagram (Figure 8b), the entire granitoid suite plots within the collisional granite field. These geochemical features support the hypothesis of the existence of a former subduction zone in the studied region or its immediate vicinity, followed by a collisional tectonic episode. This reflects a stage of continental accretion and crustal reorganization, comparable to events described in other segments of the Central African Orogenic Belt (CAOB) or the Saharan Metacraton (Abdelsalam *et al.,* 2002). The leucogranites, on the other hand, are distributed within the intraplate

granite field. They thus indicate a post-collisional tectonomagmatic reactivation and most likely mark a late phase of crustal differentiation associated with tectonic relaxation.

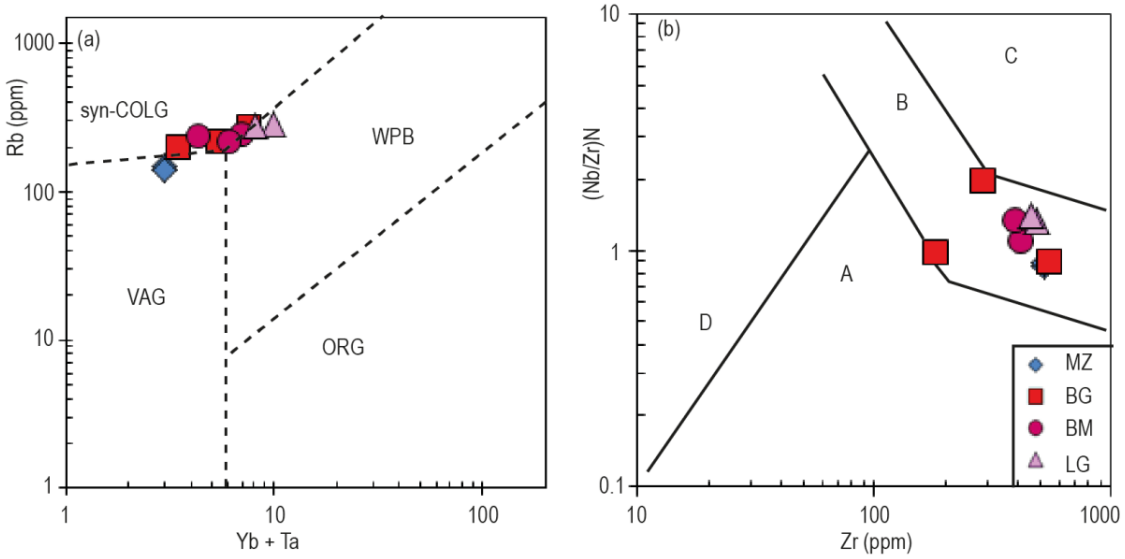

Figure 8 : Discrimination diagrams of Aboudeïa granitoïdes. (d) (Y+Nb) versus Rb (Pearce *et al.*, 1984). VAG (volcanic arc granites), COLG (collision granites), WPG (within-plate granites), and ORG (ocean-ridge granites). (c) Zr vs (Nb/Zr)N diagram of Thiéblemont and Tegyey (1994) for the granitoids of Aboudeïa. A = subduction-zone magmatic rocks; B = collision zone rocks; C = alkaline intra-plate zone rocks. Normalization to primitive mantle values from (Sun and McLennan, 1989).

CONCLUSION

Petrographic and geochemical studies conducted on the Aboudeïa granitoids provide essential insights into their source and tectonic framework. The identified facies include monzonite (Kfs + Pl + Qtz + Bt + Cpx + Amp + Sph + Epi + Ox), biotite granite (Kfs + Qtz + Pl + Bt + Ox), biotite microgranite (Qtz + Kfs + Pl + Bt + Zr + Py + Ox), and leucogranite (Kfs + Qtz + Pl + Bt + Ox). These rocks display granular to microgranular textures.

The lithological diversity observed in the study area reflects the coexistence of multiple magmatic processes associated with distinct tectonic environments. The monzonites, with shoshonitic and metaluminous affinities, originated from partial melting of metabasalts and metatonalites in a volcanic arc setting influenced by subduction. Biotite granites and biotite microgranites, characterized by a strongly potassic calc-alkaline affinity, derived from partial melting of metagreywackes and were emplaced in syn-collisional environments. Leucogranites, also characterized by a strongly potassic calc-alkaline affinity, originated from partial melting of metagreywackes, emplaced in an intraplate setting, and thus indicate a post-collisional tectonomagmatic reactivation. Overall, the magmatic evolution of these granitoids appears to have been dominated by fractional crystallization and significant crustal contamination, supporting the hypothesis of a former subduction zone followed by collisional tectonics.

ACKNOWLEDGEMENT

This study was conducted as part of the research activities led by the first author. We extend our sincere gratitude to the administrative authorities of Aboudeïa for their valuable collaboration and for authorizing the field campaigns. We thank Nabia Kounda Koko and Maxime Moyambeye for their help during field campaigns. Finally, we thank the team at ALS Geochemistry-Loughrea (Ireland) for their professionalism and commitment, which enabled the completion of geochemical analyses.

REFERENCES

Abdelsalam MG, Liégeois JP and Stern RJ (2002). The Saharan Metacraton. *Journal of African Earth Sciences*, 34, 119–136. https://doi.org/10.1016/s0899-5362(02)00013-1

Altherr FF, Holl A, Hegner E, Langer C and Kreuzer H (2000). High-potassium, calc-alkaline I-type plutonism in the European variscides: northern Vosges (France) and northern Schwarzwald (Germany). *Lithos*, 50, 51-73. https://doi.org/10.1016/s0024-4937(99)00052-3

Assadi AO, Emmanuel NN and Fadimatou YN (2022). Petrogenesis and Tectonic Setting of the Gold-Bearing Magmatic Rocks of the North-Western Melfi Massif, Central Chad. *European Journal of Environment and Earth Sciences*. 3-4, 304. https://doi.org/10.24018/ejgeo.2022.3.4.304

Baïssemia Ronang G, Gountié Dedzo M, Tcheumenak Kouémo J, Klamadji Ngarena M, Mbaguedjé D and Kwékam M (2024). Petrography and geochemical characterization of the Baïbokoum syenitic pluton (Southern Chad): implication for the magma genesis. *Acta Geochimica*, 2, 420-439. https://doi.org/10.1007/s11631-024-00733-y

Barbarin B (1999). A review of the relationships between granitoid types, their origins and their geodynamic environments. *Lithos*, 46, 605–626. https://doi.org/10.1016/s0024-4937(98)00085-1

Bessoles B and Trompette R (1980). Géologie de l'Afrique. La chaine panafricaine''«zone mobile d'Afrique centrale»'', (partie sud) et zone soudanaise. *Mémoire BRGM, Orléans (France)*, 92, 394. https://doi.org/10.1016/0012-8252(80)90092-6

Braitenberg C, Mariani P, Ebbing J and Sprlak M (2011). The enigmatic Chad lineament revisited with global gravity and gravity-gradient fields. https://doi.org/10.1144/sp357.18 , In: Van Hinsbergen DJJ, Buiter SJH, Torsvik TH, Gaina C and Webb SJ (Eds.) The Formation and Evolution of Africa: a Synopsis of 3.8 Ga of Earth History. 357. *Geological Society of London Special Publication*, pp. 329–341. https://doi.org/10.1144/sp357.1

Castaing C, Feybesse JL, Thieblemont D, Triboulet C and Chevremont P (1994). Palaeogeographical reconstructions of the Pan-African/ Brasiliano Orogen; closure of an oceanic domain or intracontinental convergence between major blocks? *Precambrian Research*, 69, 327–344. https://doi.org/10.1016/0301-9268(94)90095-7

Chappell BW and White AJR (1992). I- and S-type granites in the Lachlan Fold Belt. Transactions of the Royal Society of Edinburgh: *Earth Sciences* 83, 1–26. https://doi.org/10.1017/s0263593300007720

Chappell B and White AJR (1974). Two contrasting granite types. *Pacificn. Geology*, 8: 173–174. https://doi.org/10.1046/j.1440-0952.2001.00882.x

Diontar M, Doumnang JC, Kwékam M, Al-hadj Hamid Z, Kagou Dongmo A, Efon Awoum J and Tcheumenak Kouémo J (2020). Petrogenesis of Magnesian High-K Granitoids From Bitkine (Centrechad Massif): Major and Trace Elements Constraints. *European Journal of Environment and Earth Sciences*, 1(5). https://doi.org/10.24018/ejgeo.2020.1.5.78

Djerossem NF, Berger J, Vanderhaeghe O, Isseini M, Ganne J and Zeh A (2020). Neoproterozoic magmatic evolution of the southern Ouaddaï Massif (Chad). *Bulletin de la Société Géologique de France (BSGF)*, 191, 34. https://doi.org/10.1051/bsgf/2020032

Frost BR, Arculus RJ, Barnes CG, Collins WJ, Ellis DJ and Frost CD (2001). A geochemical classification of granitic rocks. *Journal of Petrology*, 42, 2033-2048.

Hofmann C, Courtillot V, Feraud G, Rochette P, Yirgu G, Ketefo E and Pik R (1997). Timing of the Ethiopian flood basalt event and implications for plume birth and global change. *Nature* 389 (6653), 838–841. https://doi.org/10.1038/39853

Isseini M, Hamit A and Abderamane M (2013). The tectonic and geological framework of the Mongo area, a segment of the Pan-African Guera Massif in Central Chad: evidences from field observations and remote sensing. *La Revue Scientifique du Tchad* 1, 4–12.

Isseini M, André-Mayer A, Vanderhaeghe O, Barbey P and Deloule E (2012). A-type granites from the Pan-African orogenic belt in South-Western Chad constrained using geochemistry, Sr-Nd isotopes and U-Pb geochronology. *Lithos,* 153, 39–52. https://doi.org/10.1016/j.lithos.2012.07.014

Jackson NJ and Ramsay CR (1980). What is the ‘‘Pan-African’’? A consensus is needed. *Journal of Geology*, 8, 210–211. https://doi.org/10.1130/0091-7613(1980)8<210:witpac>2.0.co;2
Kasser MY (1995). Evolution précambrienne de la région du Mayo Kebbi (Tchad). Un segment de la Chaîne Panafricaine. Thèse de Doctorat, Muséum d'Histoire Naturelle de Paris (France), p. 217
Kusnir and Moutaye (1997). Ressources minerals du Tchad: une revue. *Journal of African Earth Sciences* 24, 549–562. https://doi.org/10.1016/s0899-5362(97)00080-8
Le Maitre RW (1989). A Classification of Igneous Rocks and Glossary of Terms: Recommendations of the IUGS Subcommission on the Systematics of Igneous Rocks. *Blackwell, Oxford,* pp. 130–171.
Liégeois JP, Abdelsalam MG, Ennih N and Ouabadi A (2013). Metacraton: Nature, genesis and behavior. *Gondwana Research* 23: 220–237. https://doi.org/10.1016/j.gr.2012.02.016
Louis, P (1970). Contribution géophysique à la connaissance géologique du bassin du lac Tchad. *Bulletin ORSTOM*, 42.
Maniar PD and Piccoli PM (1989). Tectonic discrimination of granitoids. *Geological Society of American Bulletin*, 101, 635–643. https://doi.org/10.1130/0016-7606(1989)101<0635:tdog>2.3.co;2
Moyen F, Laurent O, Michou C, Chelle Couzinié S, Vanderhaeghe O, Zeh A, Villaros A and Gardien V (2017). Collision vs.subduction-related magmatism: two contrasting ways of granite formation and implications for crustal growth. *Lithos,* 277, 154–177. https://doi.org/10.1016/j.lithos.2016.09.018.
Pearce JA, Harris NBW and Tindle AG (1984). Trace Element Discrimination Diagrams for the Tectonic Interpretation of Granitic Rocks. *Journal of Petrology,* 25, 956-983. http://dx.doi.org/10.1093/petrology/25.4.956
Pearce (1975). Basalt geochemistry used to investigate past tectonic environments on Cyprus. *Tectonophysics* 25, 41-67. https://doi.org/10.1016/0040-1951(75)90010-4
Pham CT, Shellnutt JG, Yeh MW and Iizuka Y (2020). An Assessment of the Magmatic Conditions of Late Neoproterozoic Collisional and Post-collisional Granites From the Guéra Massif, South-Central Chad Front. *Earth Sciences*, 8-318. https://doi.org/10.3389/feart.2020.00318
Pouclet A, Vidal M, Doumnang JC, Vicat JP and Tchameni R (2006). Neoproterozoic crustal evolution in Southern Chad: Pan-African ocean basin closing, arc accretion and late- to post-orogenic granitic intrusion. *Journal of African Earth Sciences*, 44, 543-60. https://doi.org/10.1016/j.jafrearsci.2005.11.019
Rickwood (1989). Boundary lines within petrologic diagrams which use oxides of major and minor elements. *Lithos* 22, 247–264. https://doi.org/10.1016/0024-4937(89)90028-5
Seguem N, Diondoh M, Kepnamou AD, Mama N, Sami M, Alexandre G and Emmanuel EG (2022). Petrography and Geochemistry of Baibokoum-Touboro-Ngaoundaye Granitoids on the Chad-Cameroon-RCA Borders (Adamawa-Yade Domain). *Open Journal of Geology,* 12, 136-155. https://doi.org/10.4236/ojg.2022.122007
Shellnutt JG, Pham NHT, Yeh MW and Lee TY (2019). “Two series of Ediacaran collision-related granites in the Guéra Massif (Chad): tectonomagmatic constraints on the terminal collision of the eastern Central African Orogenic Belt. *Precambrian Research*, 347, 105823. https://doi.org/10.1016/j.precamres.2020.105823
Shellnutt JG, Yeh MW, Lee TY, Iizuka Y, Pham NHT and Yang CC (2018). The origin of Late Ediacaran post-collisional granites near the Chad Lineament, Saharan Metacraton, south-central Chad. *Lithos* 304, 450–467. https://doi.org/10.1016/j.lithos.2018.02.020
Shellnutt JG, Pham TNH, Denyszyn S, Yeh MW and Lee TY (2017). Timing of collisional and post-collisional Pan-African Orogeny silicic magmatism in south-central Chad. *Precambrian Research,* 301, 113–123. doi: 10.1016/j.precamres.2017.08.021
Shellnutt JG, Lee TY, Torng PK, Yang CC and Lee YH (2016). Late Cretaceous intraplate silicic volcanism in the Lake Chad region: a northern extension of the Cameroon volcanic line? *Geochemistry, Geophysics, Geosystems* 17, 2803–2824. https://doi.org/10.1002/2016GC006298

Sun SS and McLennan WF (1989). Rare earth elements in sedimentary rocks: influence of provenance and sedimentary processes. In: Lipin BR, MacKay GA (eds) Geochemistry and mineralogy of rare earth elements. *Mineral Society of America, Chantilly*, 169-200. https://doi.org/10.1515/9781501509032-010
Thiéblemont D and Tegyey M (1994). Une discrimination géochimique des Roches différenciées témoin de la diversité d'origine et de situation Tectonique des magmas calco-alcalins. Comptes Rendus de l'Académie Des Sciences, 319, 87-94.
Thompson RN, Morrison MA, Hendry GL and Parry SJ (1984). An assessment of relative roles of crust and mantle in magma genesis: an elemental approach. *Philosophical Transactions of the Royalty Society of London, Series*, *A*. 310: 549–590.
Wu DQ, Sun FY, Pan ZC and Tian N (2020). Geochronology, geochemistry, and Hf isotopic compositions of Triassic igneous rocks in the easternmost segment of the East Kunlun Orogenic Belt, NW China: implications for magmatism and tectonic evolution. *Internationale Geology Revew*. 1–19. https://doi.org/10.1080/00206814.2020.1740895